

Supplementary File to “External Prior Guided Internal Prior Learning for Real-World Noisy Image Denoising”

Jun Xu¹, *Student Member, IEEE*, Lei Zhang¹, *Fellow, IEEE*, and David Zhang², *Fellow, IEEE*

¹Department of Computing, The Hong Kong Polytechnic University, Hong Kong SAR, China

²School of Science and Engineering, The Chinese University of Hong Kong (Shenzhen), Shenzhen, China

In this supplementary file, we provide:

- 1) More results on the 15 cropped real-world noisy images in dataset [1];
- 2) More results on the 60 cropped real-world noisy images in dataset [1];
- 3) More results on the 1000 cropped real-world noisy images in dataset [2];
- 4) More results on the 100 cropped real-world noisy images in our new dataset.

I. MORE RESULTS ON THE 15 CROPPED REAL-WORLD NOISY IMAGES IN DATASET [1]

In this section, we provide more comparisons of the proposed method with the state-of-the-art denoising methods on the 15 cropped real-world noisy images used in [1]. In this dataset, each scene was shot 500 times under the same camera and camera setting. The mean image of the 500 shots is roughly taken as the “ground truth”, with which the PSNR and SSIM [3] can be computed. The average SSIM results of GAT-BM3D [4], CBM3D [5], WNNM [6], TID [7], MLP [8], CSF [9], TNRD [10], DnCNN [11], NI [12], NC [13], [14], CC [1], and the proposed method are listed in Table I. As can be seen from Figures 1-2, our proposed method achieves visually more pleasing results than the competing methods.

TABLE I: SSIM [3] results of different methods on 15 cropped real-world noisy images used in [1].

Setting	GAT-BM3D	CBM3D	WNNM	TID	MLP	CSF	TNRD	DnCNN	NI	NC	CC	Ours
Canon 5D Mark III ISO = 3200	0.9126	0.9778	0.9673	0.9515	0.9695	0.9434	0.9742	0.9389	0.9600	0.9689	0.9678	0.9813
	0.8427	0.9552	0.9210	0.9041	0.9458	0.9011	0.9491	0.8989	0.9308	0.9427	0.9359	0.9572
	0.8017	0.9660	0.9110	0.9354	0.9599	0.9037	0.9617	0.9182	0.9463	0.9476	0.9478	0.9643
Nikon D600 ISO = 3200	0.7845	0.9330	0.9281	0.8913	0.9481	0.8792	0.9494	0.9123	0.9413	0.9497	0.9484	0.9535
	0.9028	0.9168	0.9432	0.8605	0.9469	0.9261	0.9499	0.8932	0.9251	0.9398	0.9293	0.9461
	0.9806	0.9313	0.9737	0.8632	0.9726	0.9763	0.9742	0.8708	0.9481	0.9588	0.9799	0.9683
Nikon D800 ISO = 1600	0.8791	0.9339	0.9417	0.8832	0.9543	0.9148	0.9572	0.9060	0.9506	0.9533	0.9575	0.9620
	0.9534	0.9383	0.9748	0.8772	0.9743	0.9674	0.9774	0.8943	0.9615	0.9591	0.9767	0.9779
	0.8795	0.9277	0.9311	0.8451	0.9354	0.9035	0.9410	0.8735	0.9229	0.9406	0.9427	0.9531
Nikon D800 ISO = 3200	0.9526	0.8866	0.9656	0.8356	0.9533	0.9654	0.9569	0.8463	0.9101	0.9466	0.9637	0.9613
	0.9078	0.8928	0.9416	0.7761	0.9381	0.9354	0.9394	0.8755	0.9194	0.9309	0.9477	0.9521
	0.9707	0.8430	0.9664	0.7882	0.9548	0.9712	0.9576	0.7204	0.9001	0.9070	0.9544	0.9512
Nikon D800 ISO = 6400	0.8909	0.7952	0.9188	0.7118	0.8914	0.9259	0.8966	0.7847	0.7781	0.9024	0.9206	0.8958
	0.8328	0.8613	0.9050	0.7995	0.9137	0.9127	0.9142	0.8259	0.8649	0.9141	0.9369	0.9242
	0.7773	0.8363	0.8818	0.7717	0.8958	0.8494	0.8960	0.7936	0.8295	0.8847	0.9118	0.9092
Average	0.8846	0.9063	0.9381	0.8463	0.9436	0.9250	0.9463	0.8635	0.9126	0.9364	0.9481	0.9505

II. MORE RESULTS ON THE 60 CROPPED REAL-WORLD NOISY IMAGES IN DATASET [1]

In this section, we provide more comparisons of the proposed method with the state-of-the-art denoising methods on the 60 real-world noisy images cropped from [1]. In this dataset, each scene was shot 500 times under the same camera and camera setting. The mean image of the 500 shots is roughly taken as the “ground truth”, with which the PSNR and SSIM can be computed. The average SSIM results of GAT-BM3D [4], CBM3D [5], WNNM [6], MLP [8], CSF [9], TNRD [10], DnCNN [11], NI [12], NC [13], [14], and the proposed method are listed in Table II (CC is not compared since the code of [1] is not available). As can be seen from Figures 3-4, our proposed method achieves visually more pleasing results than the competing methods.

TABLE II: Average SSIM [3] results of different methods on 60 real-world noisy images cropped from [1].

Methods	GAT-BM3D	CBM3D	WNNM	MLP	CSF	TNRD	DnCNN	NI	NC	Ours
SSIM	0.9331	0.9251	0.9633	0.9653	0.9598	0.9670	0.8873	0.9241	0.9514	0.9691

III. MORE RESULTS ON THE 1000 CROPPED REAL-WORLD NOISY IMAGES IN DATASET [2]

In this section, we give more visual comparisons of the competing methods on the 1000 cropped real-world noisy images in [2]. In this dataset, each scene was shot twice, one at a high ISO value and the other at a low ISO value. The image captured at low ISO value (usually 100 or 125) is roughly taken as the “ground truth”, with which the PSNR and SSIM [3] can be computed. The average SSIM results of GAT-BM3D [4], CBM3D [5], WNNM [6], MLP [8], CSF [9], TNRD [10], DnCNN [11], NI [12], NC [13], [14], and the proposed method are listed in Table III (CC is not compared since the code of [1] is not available). As can be seen from Figures 5-8, our proposed method achieves visually more pleasing results than the competing methods.

TABLE III: Average SSIM [3] results of different methods on 1000 real-world noisy images cropped from the dataset [2].

Methods	GAT-BM3D	CBM3D	WNNM	MLP	CSF	TNRD	DnCNN	NI	NC	Ours
SSIM	0.7564	0.7773	0.8012	0.8201	0.8128	0.8271	0.7897	0.8778	0.9013	0.9101

IV. MORE RESULTS ON THE 100 CROPPED REAL-WORLD NOISY IMAGES IN OUR NEW DATASET

In this section, we provide more comparisons of the proposed method with the state-of-the-art denoising methods on the 100 real-world noisy images cropped from the new dataset we constructed. In this dataset, each scene was shot 500 times under the same camera and camera setting. The mean image of the 500 shots is roughly taken as the “ground truth”, with which the PSNR and SSIM can be computed. The average SSIM results of GAT-BM3D [4], CBM3D [5], WNNM [6], MLP [8], CSF [9], TNRD [10], DnCNN [11], NI [12], NC [13], [14], and the proposed method are listed in Table IV (CC is not compared since the code of [1] is not available). As can be seen from Figures 9-10, our proposed method achieves visually more pleasing results than the competing methods.

TABLE IV: Average SSIM [3] results of different methods on 100 real-world noisy images cropped from our new dataset.

Methods	GAT-BM3D	CBM3D	WNNM	MLP	CSF	TNRD	DnCNN	NI	NC	Ours
SSIM	0.8881	0.9494	0.9290	0.9453	0.9398	0.9486	0.8852	0.9190	0.9356	0.9529

REFERENCES

- [1] S. Nam, Y. Hwang, Y. Matsushita, and S. J. Kim. A holistic approach to cross-channel image noise modeling and its application to image denoising. *IEEE Conference on Computer Vision and Pattern Recognition (CVPR)*, pages 1683–1691, 2016. [1](#), [2](#), [3](#), [4](#), [5](#), [6](#), [11](#), [12](#)
- [2] T. Plötz and S. Roth. Benchmarking denoising algorithms with real photographs. In *CVPR*, 2017. [1](#), [2](#), [7](#), [8](#), [9](#), [10](#)
- [3] Z. Wang, A. C. Bovik, H. R. Sheikh, and E. P. Simoncelli. Image quality assessment: from error visibility to structural similarity. *IEEE Transactions on Image Processing*, 13(4):600–612, 2004. [1](#), [2](#)
- [4] M. Makitalo and A. Foi. Optimal inversion of the generalized anscombe transformation for poisson-gaussian noise. *IEEE Transactions on Image Processing*, 22(1):91–103, 2013. [1](#), [2](#)
- [5] K. Dabov, A. Foi, V. Katkovnik, and K. Egiazarian. Image denoising by sparse 3-D transform-domain collaborative filtering. *IEEE Transactions on Image Processing*, 16(8):2080–2095, 2007. [1](#), [2](#)
- [6] S. Gu, L. Zhang, W. Zuo, and X. Feng. Weighted nuclear norm minimization with application to image denoising. *IEEE Conference on Computer Vision and Pattern Recognition (CVPR)*, pages 2862–2869, 2014. [1](#), [2](#), [3](#), [4](#), [5](#), [6](#), [7](#), [8](#), [9](#), [10](#), [11](#), [12](#)
- [7] Enming Luo, Stanley H Chan, and Truong Q Nguyen. Adaptive image denoising by targeted databases. *IEEE Transactions on Image Processing*, 24(7):2167–2181, 2015. [1](#)
- [8] H. C. Burger, C. J. Schuler, and S. Harmeling. Image denoising: Can plain neural networks compete with BM3D? *IEEE Conference on Computer Vision and Pattern Recognition (CVPR)*, pages 2392–2399, 2012. [1](#), [2](#), [7](#), [8](#), [9](#), [10](#)
- [9] U. Schmidt and S. Roth. Shrinkage fields for effective image restoration. *IEEE Conference on Computer Vision and Pattern Recognition (CVPR)*, pages 2774–2781, June 2014. [1](#), [2](#), [5](#), [6](#), [7](#), [8](#), [9](#), [10](#), [11](#), [12](#)
- [10] Y. Chen, W. Yu, and T. Pock. On learning optimized reaction diffusion processes for effective image restoration. *IEEE Conference on Computer Vision and Pattern Recognition (CVPR)*, pages 5261–5269, 2015. [1](#), [2](#), [3](#), [4](#), [5](#), [6](#), [7](#), [8](#), [9](#), [10](#), [11](#), [12](#)
- [11] K. Zhang, W. Zuo, Y. Chen, D. Meng, and L. Zhang. Beyond a Gaussian denoiser: Residual learning of deep cnn for image denoising. *IEEE Transactions on Image Processing*, 2017. [1](#), [2](#), [3](#), [4](#), [5](#), [6](#), [7](#), [8](#), [9](#), [10](#), [11](#), [12](#)
- [12] Neatlab ABSsoft. Neat Image. <https://ni.neatvideo.com/home>. [1](#), [2](#), [3](#), [4](#), [5](#), [6](#), [7](#), [8](#), [9](#), [10](#), [11](#), [12](#)
- [13] M. Lebrun, M. Colom, and J.-M. Morel. Multiscale image blind denoising. *IEEE Transactions on Image Processing*, 24(10):3149–3161, 2015. [1](#), [2](#), [3](#), [4](#), [5](#), [6](#), [7](#), [8](#), [9](#), [10](#), [11](#), [12](#)
- [14] M. Lebrun, M. Colom, and J. M. Morel. The noise clinic: a blind image denoising algorithm. <http://www.ipol.im/pub/art/2015/125/>. Accessed 01 28, 2015. [1](#), [2](#), [3](#), [4](#), [5](#), [6](#), [7](#), [8](#), [9](#), [10](#), [11](#), [12](#)
- [15] K. Dabov, A. Foi, V. Katkovnik, and K. Egiazarian. Color image denoising via sparse 3D collaborative filtering with grouping constraint in luminance-chrominance space. *IEEE International Conference on Image Processing (ICIP)*, pages 313–316, 2007. [3](#), [4](#), [5](#), [6](#), [7](#), [8](#), [9](#), [10](#), [11](#), [12](#)

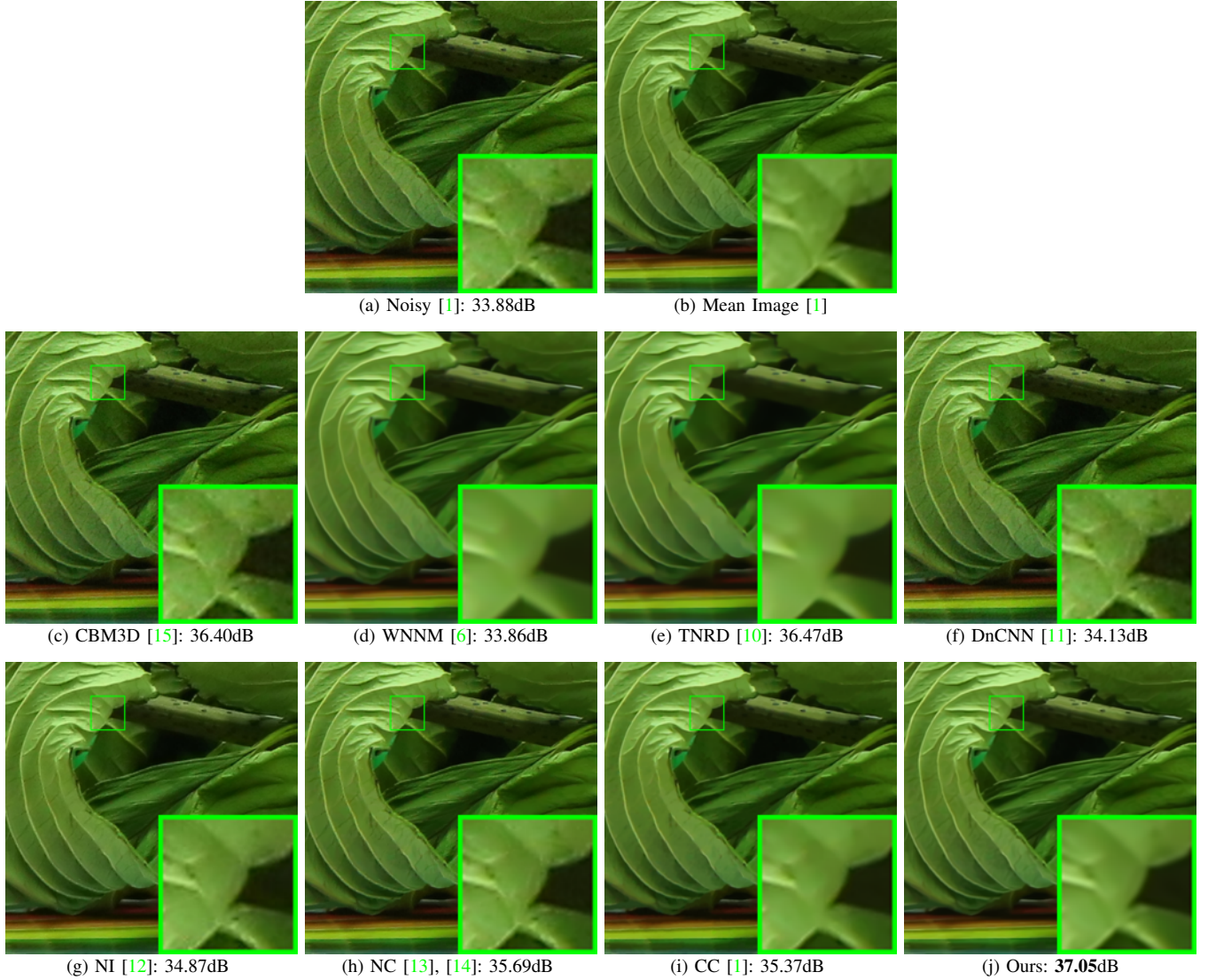


Fig. 1: Denoised images of a region cropped from the real-world noisy image “Canon 5D Mark 3 ISO 3200 2” [1] by different methods. The images are better to be zoomed-in on screen.

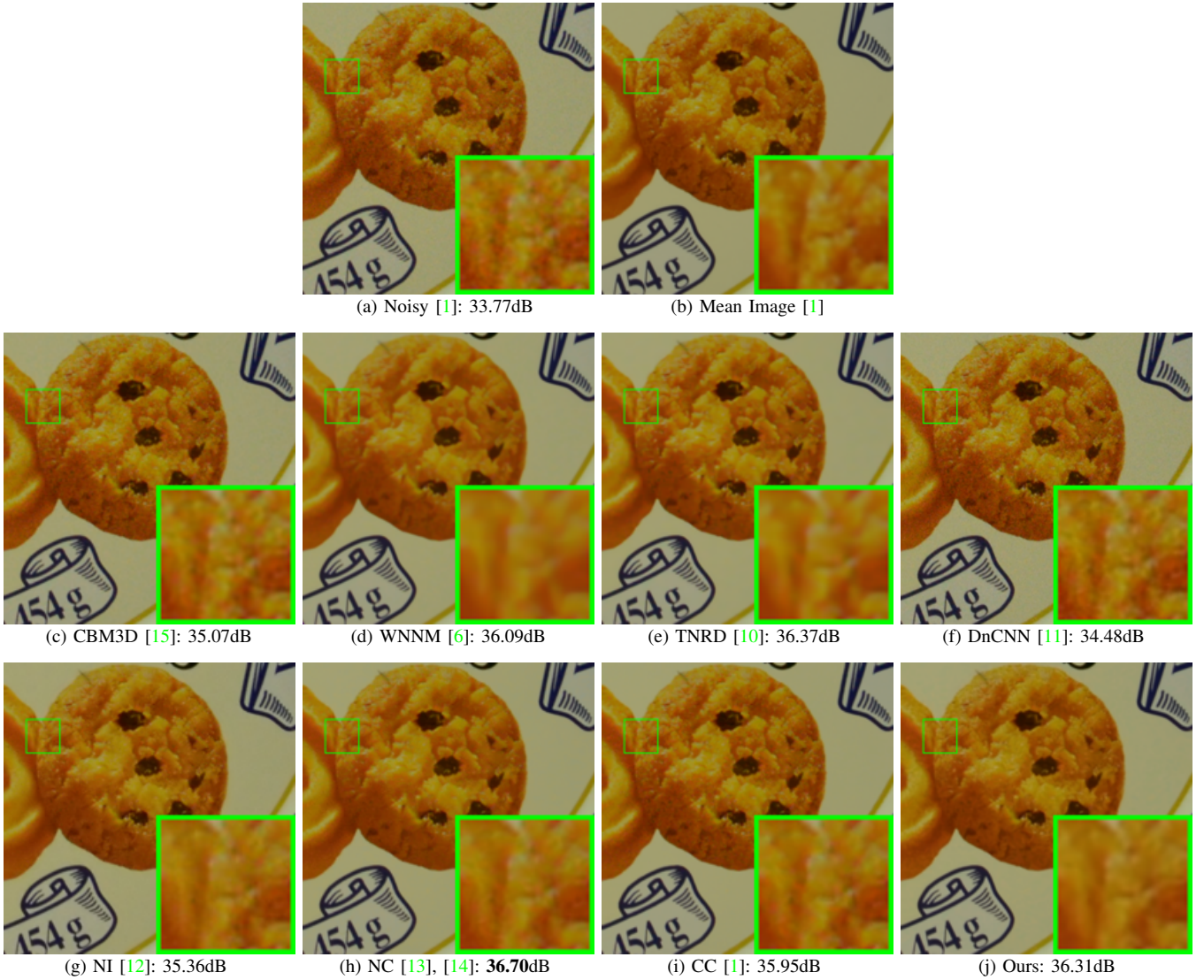


Fig. 2: Denoised images of a region cropped from the real-world noisy image “Nikon D600 ISO 3200 2” [1] by different methods. The images are better to be zoomed-in on screen.



Fig. 3: Denoised images of a region cropped from the real-world noisy image “Nikon D800 ISO 1600 B2” [1] by different methods. The images are better viewed by zooming in on screen.

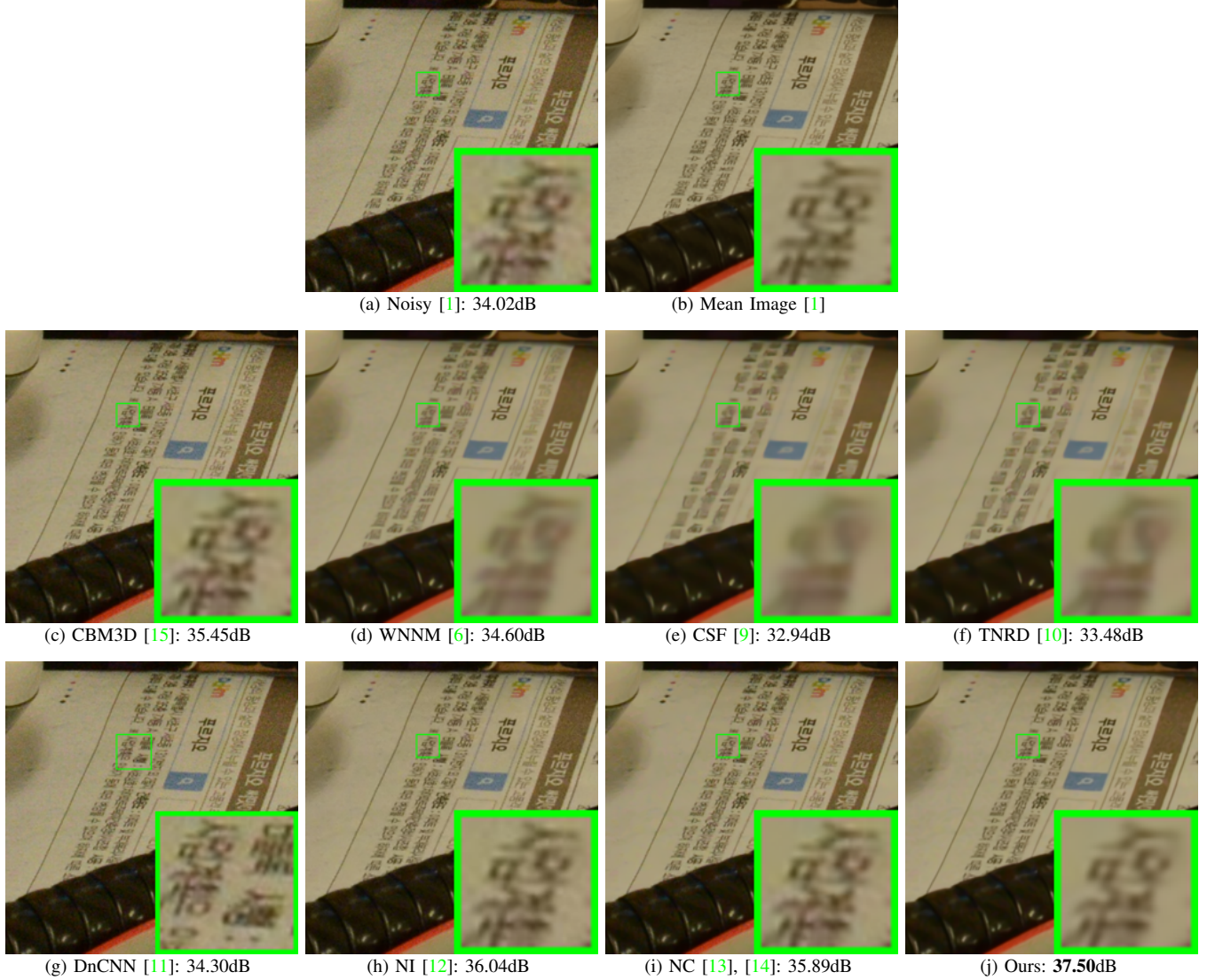


Fig. 4: Denoised images of a region cropped from the real-world noisy image “Nikon D800 ISO 3200 A1” [1] by different methods. The images are better viewed by zooming in on screen.

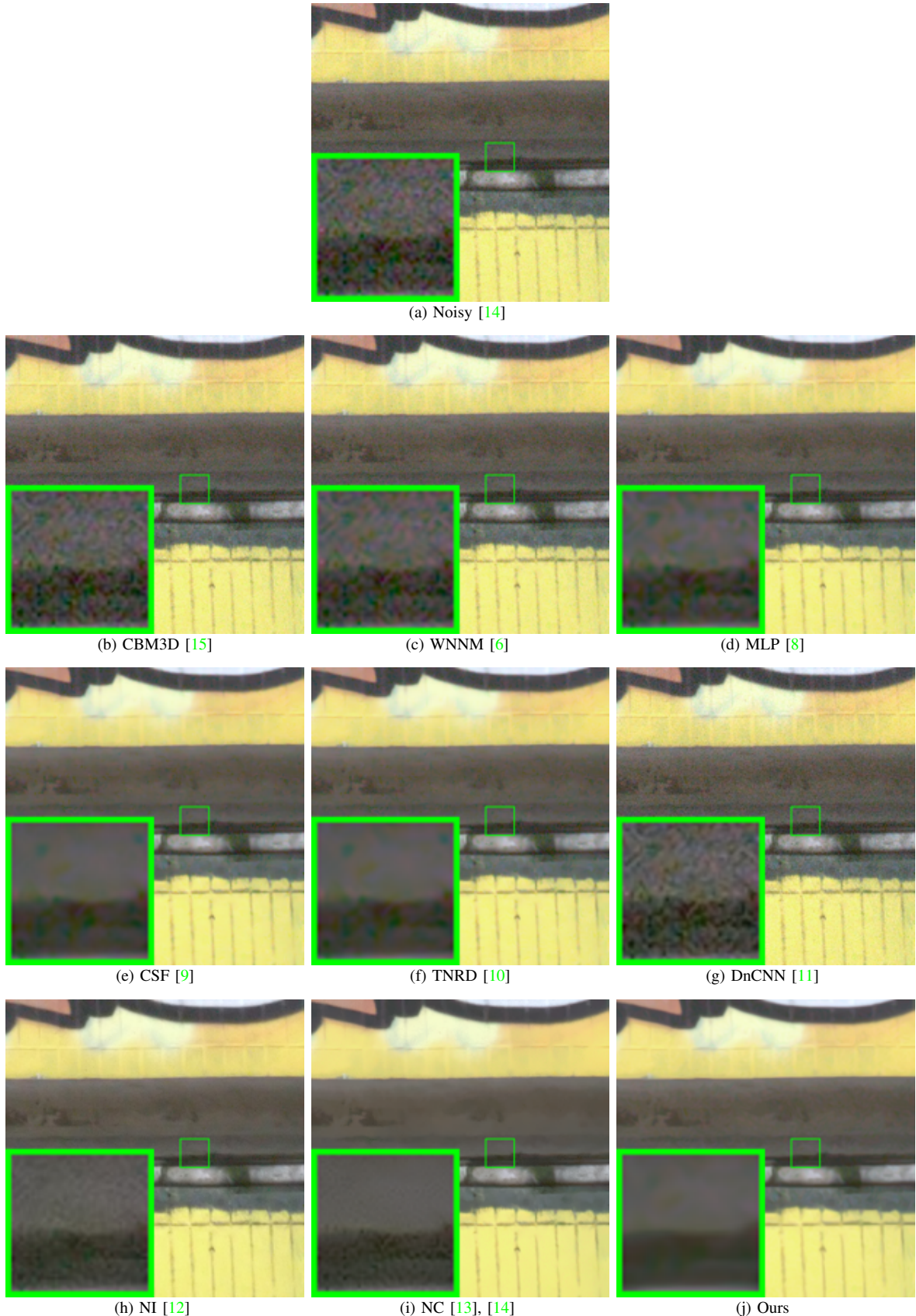


Fig. 5: Denoised images by different methods of the real-world noisy image “0002_10” captured by a Huawei Nexus 6P phone [2]. Note that the ground-truth clean image of the noisy input is not publicly released yet.

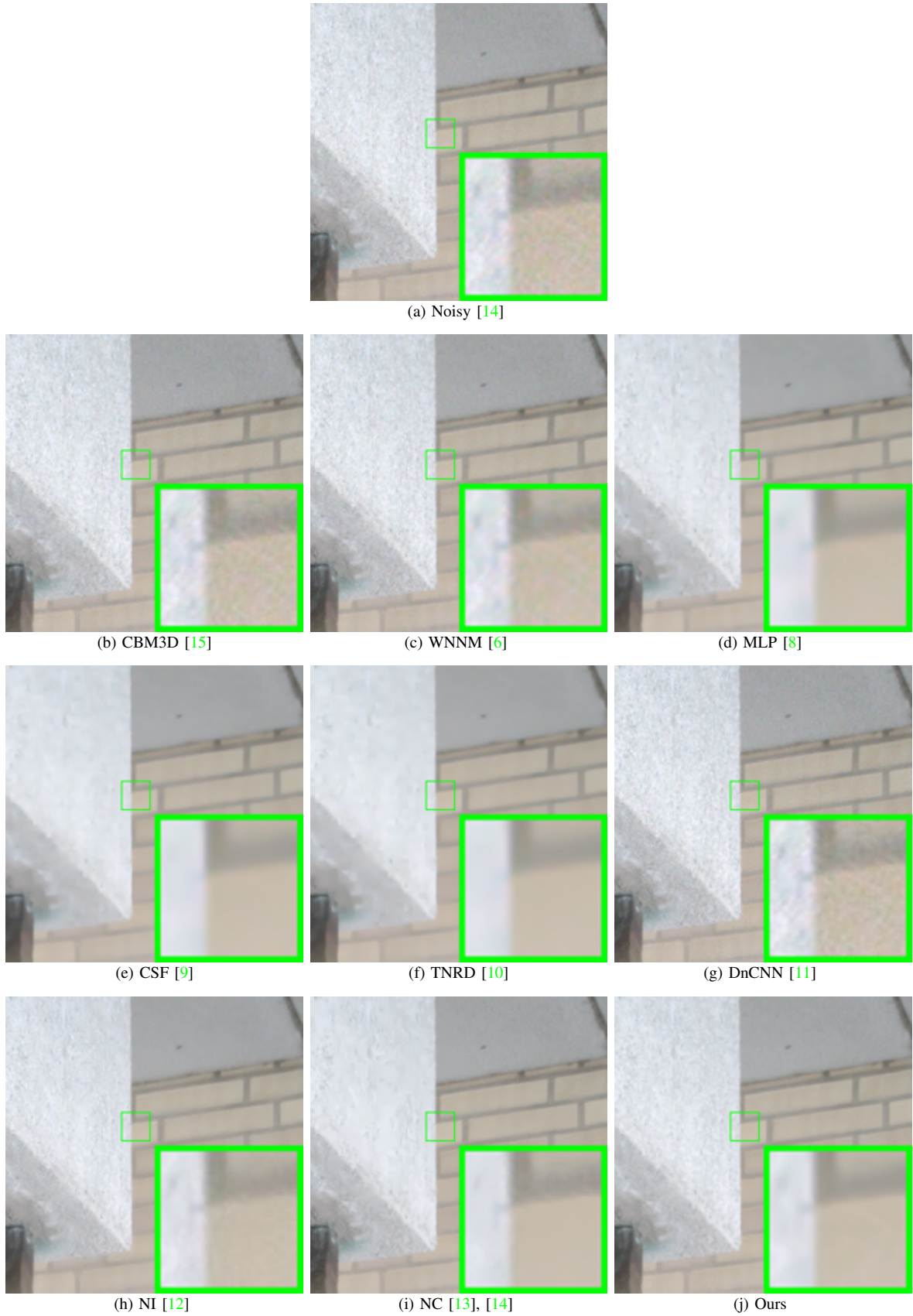


Fig. 6: Denoised images by different methods of the real-world noisy image “0003_5” captured by a Huawei Nexus 6P phone [2]. Note that the ground-truth clean image of the noisy input is not publicly released yet.

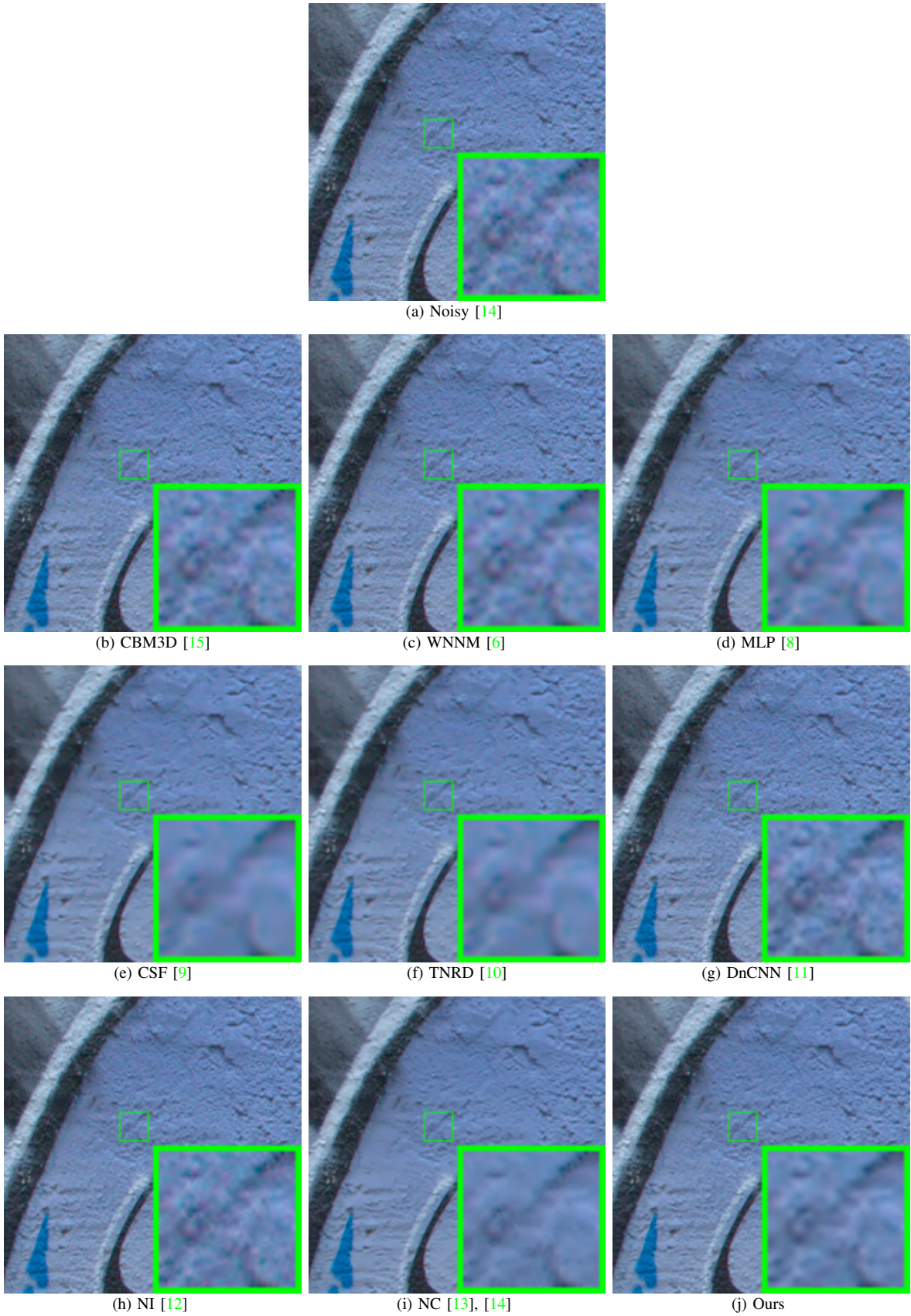


Fig. 7: Denoised images by different methods of the real-world noisy image “0006_18” captured by a Sony A7R camera [2]. Note that the ground-truth clean image of the noisy input is not publicly released yet.

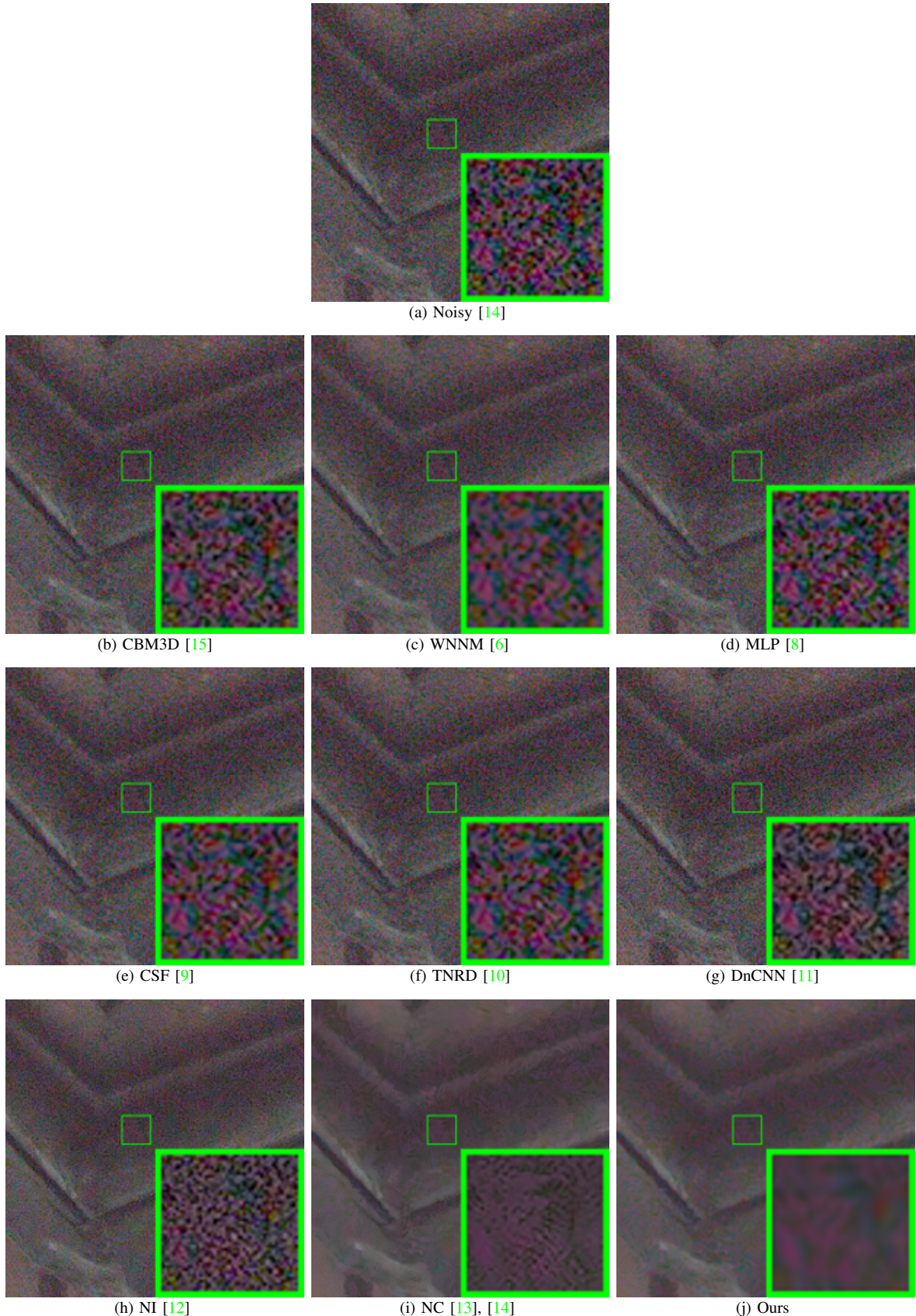


Fig. 8: Denoised images by different methods of the real-world noisy image “0049_4” captured by a Huawei Nexus 6P phone [2]. Note that the ground-truth clean image of the noisy input is not publicly released yet.

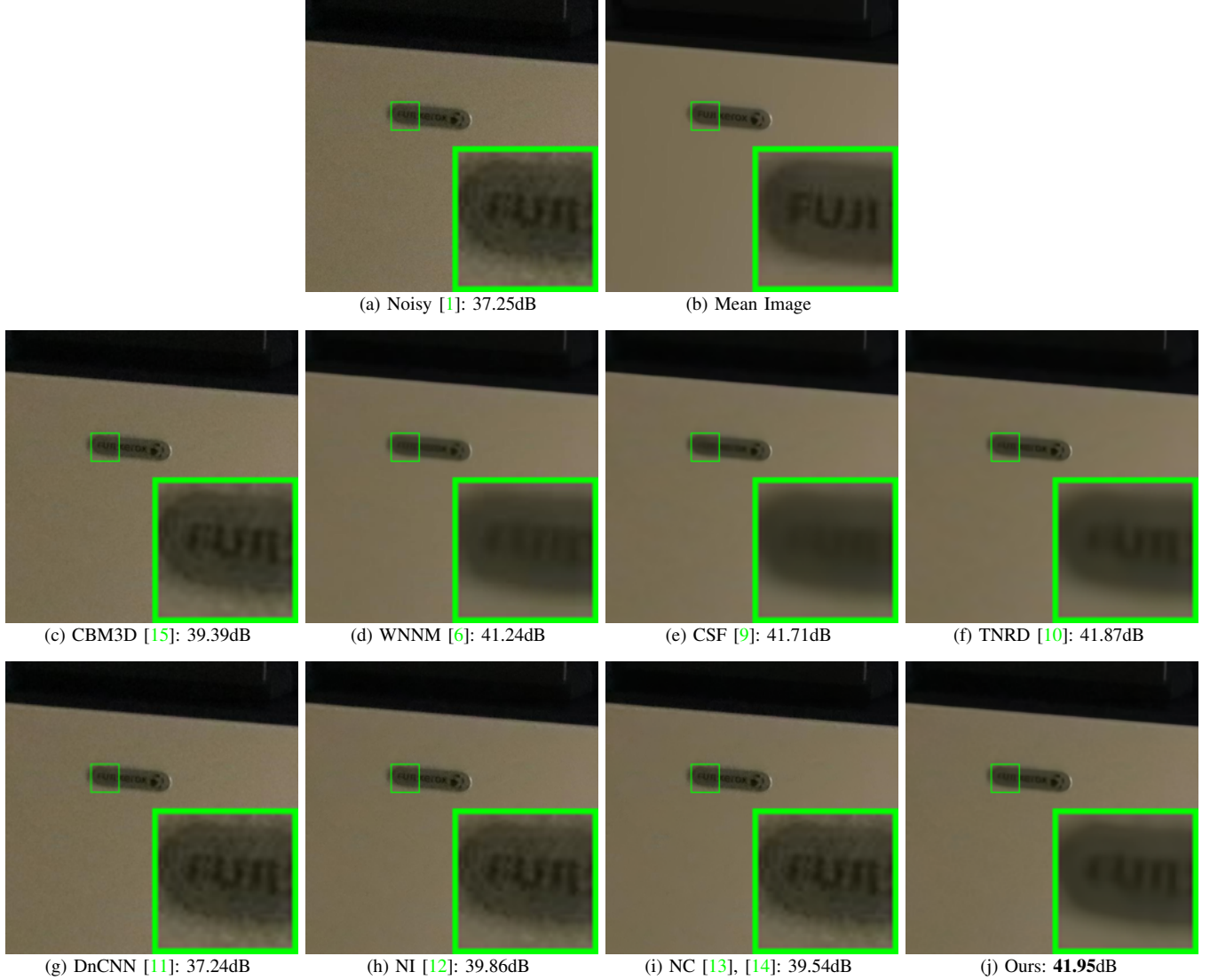


Fig. 9: Denoised images of a region cropped from the real-world noisy image “Canon 80D ISO 12800 IMG2360” in our new dataset by different methods. The images are better viewed by zooming in on screen.

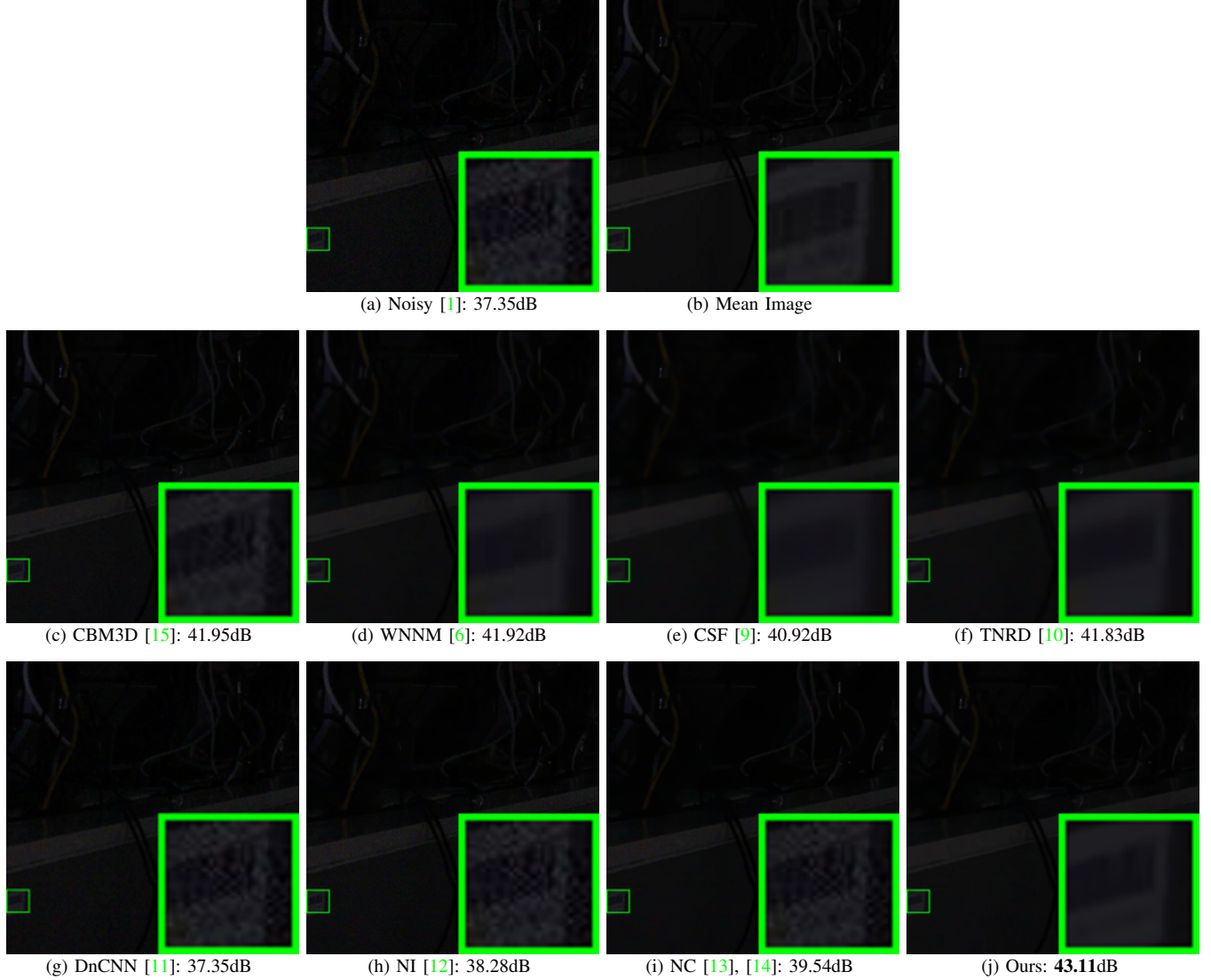


Fig. 10: Denoised images of a region cropped from the real-world noisy image “SONY A7II ISO 6400 DSC03017” in our new dataset by different methods. The images are better viewed by zooming in on screen.